



Study of enhancement in the dielectric and electrical properties of WO₃-doped LiF nano-composite

Ritu Verma^{1,2}, Surya Prakash Tiwari¹, Reena Kumari¹, and Ritu Srivastava^{1,*}

¹Advanced Material Devices Division, CSIR-National Physical Laboratory, Dr. K. S. Krishnan Road, New Delhi 110012, India

²Academy of Scientific and Innovative Research (AcSIR), CSIR-National Physical Laboratory Campus, New Delhi, India

Received: 9 June 2017

Accepted: 27 November 2017

Published online:

7 December 2017

© Springer Science+Business Media, LLC, part of Springer Nature 2017

ABSTRACT

We report the dielectric and electrical behavior of thermally evaporated lithium fluoride (LiF)–tungsten trioxide (WO₃) (x wt% WO₃-doped LiF; $x = 0, 1, 3, 5, 7, 10$) nano-composite thin films at room temperature over a wide range of frequencies from 0.1 Hz to 1 MHz. Among the various doping concentrations of WO₃, the 5 wt% WO₃-doped LiF nano-composite thin film reaches to the maximum dielectric constant ~ 25 , compared with those of pure LiF ~ 9 thin film. The electrical studies of the films have been done by complex impedance spectroscopy and show the presence of grain and grain boundaries contribution in the films for all doping concentrations. The relaxation behavior in the nano-composite films has been observed in the dielectric curve at low frequencies which is superimposed by electrode polarization. The non-Debye type of relaxation in the films has been observed in the impedance and modulus curve. The peaks appearing at low frequencies for each doping concentration in loss tangent spectrum show the presence of relaxing dipoles in the films. An increment in the ac conductivity has been observed with doping concentration up to 5%. The ac conductivity curves obey the jump relaxation power law where an electrode polarization effect can be seen at low-frequency region.

Introduction

Over a past few decades, organic field-effect transistors (OFETs) have attracted attention of the researchers due to their low cost and large area electronic applications such as displays [1, 2], sensors [3, 4] and wearable electronic [5]. Various research has been investigated to improve the characteristics of organic semiconductors for their application in high-performance organic electronic devices [6], but

recently attention has been given toward the development of high- k gate insulators to enable low voltage operation with low electrical leakage, minimum density of surface traps and highly smooth surface for the growth of active organic semiconductor layer [7]. For OFET applications, many gate dielectrics like poly(4-vinyl phenol) (PVP), benzocyclobutene (BCB), poly(methyl methacrylate) (PMMA) have been successfully demonstrated; however, the operating voltages remain high due to their low dielectric

Address correspondence to E-mail: ritu@nplindia.org

constant. Poly(vinylidene fluoride) (PVDF) and cyanoethyl pullulan (CEP) have a high dielectric constant, but suffer from disadvantages of having poor semiconductor–dielectric interface and high curing temperature, respectively [7, 8]. Polymer such as poly(vinyl alcohol) (PVA) and PVP contains hydroxyl groups which increase the number of trapping sites at the semiconductor/dielectric interface, which caused a large hysteresis in the transfer characteristics [9] of OFETs. Hence, to overcome the disadvantages of low dielectric constant and high leakage current of the gate dielectric, the study of nano-composite gate dielectrics is necessary due to their simple processing, low cost and excellent properties, such as low dielectric loss and low leakage current. OFETs fabricated with nano-composite gate dielectric showed improved transistor characteristics compared to the single gate electric devices [10]. Hence, for the development and practical application of OFET devices, nano-composite dielectrics which can provide a high-quality interface, high dielectric constant, low leakage current and low voltage operation is required.

In this work, the MIM device of LiF–WO₃ nano-composite thin films with different doping concentration of WO₃ along with its electrical and dielectric characteristics has been studied for the application of OFETs. Here LiF has been chosen because it has been widely used as gate dielectric for OFETs [11, 12] and can be easily fabricated by thermal evaporation technique. LiF has a dielectric constant (~ 9) and band gap (13.6 eV) which can provide high capacitance to the device. In the doping content, WO₃ has been chosen because WO₃ is one of the most interesting materials, which shows a wide variety of novel properties in thin film form which is useful for advanced microelectronic applications [13]. The WO₃-doped LiF nano-composite shows enhanced dielectric constant and electrical properties as compared to pure LiF and can be used in the field of organic semiconductor devices. The study of the x wt% WO₃-doped LiF nano-composite thin films has not been done so far in terms of dielectric and electrical characterization.

Materials and methods

In this study, MIM device has been fabricated on glass substrate where indium tin oxide (ITO) is considered as bottom contact where as Al is considered

as top contact and x wt% WO₃-doped LiF thin film was sandwiched between these two contacts. The ITO-coated glass substrates with sheet resistance of 20 ohms per unit area were purchased from Vin Karola, USA. The substrates were patterned of 2 mm wide strip and ultrasonically cleaned by dipping them into DI Water, Acetone, TCE and propan-2-ol solvents for 20 min each. Annealing was done after cleaning of the substrates in vacuum oven at 120 °C for 30 min. The annealed substrates were immediately loaded into a thermal evaporation coating unit by avoiding any exposure to ambient air for fabrication of devices. The MIM device structure is ITO (120 nm)/ x wt% WO₃-doped LiF (120 nm)/Al (150 nm). After loading the substrate, the dielectric material and Al film are evaporated by physical vapor deposition method. The base pressure for the fabrication of both layers was 5×10^{-6} mbar. The evaporation rate was 0.5–1 Å/s for the dielectric layer and 2–4 Å/s for Al. The device area for this structure was 2 mm \times 2 mm. Thickness of each layer was measured by quartz crystal thickness monitor Model DTM-101 and examined by spectroscopy ellipsometry (Woollam 2000). All materials the WO₃ (99.9%), LiF (99.98%) and Al (99.9%) are purchased from Sigma-Aldrich and were used directly as such. WO₃-doped LiF with different concentration has been prepared by physical mixing. The electrical properties of MIM device were determined by ac impedance spectroscopy using Solartron 1260 impedance analyzer over a frequency range from 0.1 to 10⁶ Hz. The crystallite structure of the nano-composite thin films was examined by grazing incidence X-ray diffraction (GIXRD) techniques (PANalytical X'Pert PRO MRD system) with CuK α radiation ($\lambda = 1.5405$ Å) in a wide range of Bragg angles 2θ ($35^\circ \leq 2\theta \leq 70^\circ$). FESEM-Carl Zeiss, Supra 40 VP has been used to study the surface morphology characterization.

Results and discussion

Figure 1a–g shows the X-ray diffraction of all WO₃-doped LiF nano-composite thin films with different doping concentration and pure WO₃ thin film deposited on Si substrate at room temperature. For 0 wt% WO₃-doped LiF, it is found to be highly crystalline and reflections corresponding to the LiF crystal planes (111), (200), and (220) were recognized at an angle of 38.7°, 45.0° and 65.6°, respectively [14],

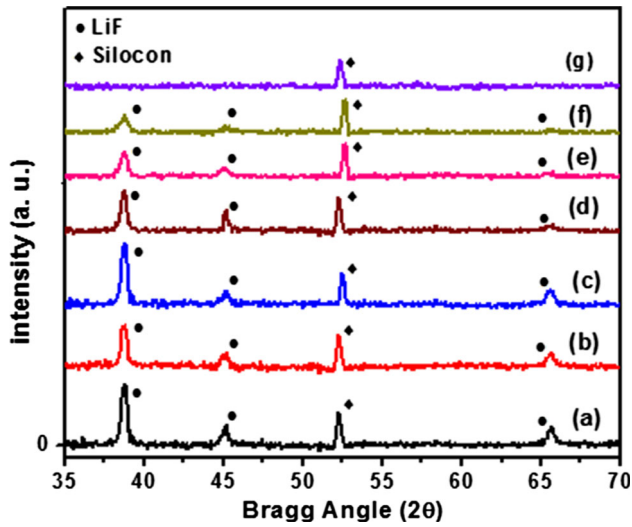


Figure 1 XRD pattern of the WO₃-doped LiF nano-composite thin films at different concentrations of WO₃: (a) 0%, (b) 1%, (c) 3%, (d) 5%, (e) 7%, (f) 10%, (g) 100%.

with no detectable crystalline impurity phases present. For other doping concentrations (Fig. 1b–f), same peaks have been observed as 0 wt% WO₃-doped LiF (Fig. 1a) and no peaks have been observed for 100 wt% WO₃-doped LiF (Fig. 1g). A comparison of all these patterns indicates no extra peak shifts in the 1 wt% WO₃-doped LiF–10 wt% WO₃-doped LiF thin film other than peaks of 0 wt% WO₃-doped LiF thin film. It can be seen that crystalline nature of the 0 wt% WO₃-doped LiF thin film decreases by increasing the doping concentration of WO₃ in the host of LiF (Fig. 1b–f). This reduction in crystalline nature of the films can be due to the amorphous behavior of the WO₃ film. It is reported that film as-deposited by thermal evaporation of WO₃ shows amorphous behavior; hence, no peak can be seen in Fig. 1g for WO₃ deposited film [15, 16]. The peak at 52.5° is due to the Si lattice from the substrate.

Figure 2a–f shows the FESEM images of all WO₃-doped LiF nano-composite thin film with different doping concentration deposited on Si substrate. It can be seen from the images that WO₃ content increases in LiF with doping of WO₃ up to 5%, which can be the possible reason for the increment behavior of electrical and dielectric properties of nano-composite. Hence 5 wt% WO₃-doped LiF thin film nano-composite shows the best composite for our analysis. It has also been seen that with further increment of WO₃ content (i.e., > 5 wt%), the grain size of WO₃ transformed into bulk form and gets agglomerated in

the matrix and this agglomeration can be the possible reason for the reduction in electrical and dielectric properties of nano-composite. This agglomerated matrix can be seen the inset image of Fig. 2f. Hence, the interfacial area per unit volume and inter-particle distance may decrease. This decreases the average polarization associated with the particles resulting in the further decrement of dielectric constant and ac conductivity as well as increment of tangent loss.

Figure 3 shows the capacitance value of LiF–WO₃ nano-composite thin films at different doping concentration as a function of frequency. It can be seen that capacitance of the LiF has been increased with increase in doping concentration up to 5%. The dielectric constant of the films has been calculated by the following formula, and the calculated values of dielectric constant are shown in Table 1

$$C_i = \frac{k\epsilon_0 A}{d}, \tag{1}$$

where C_i is the measured capacitance of the specimen in Farad (F), d is thickness of the film, ϵ_0 is the permittivity of free space (8.85×10^{-12} F/m), A is the area of the device, and k is dielectric constant of the material.

The ϵ' and ϵ'' are the real and imaginary part of the dielectric constant, which represents the amount of energy stored in a dielectric material as polarization and energy loss, respectively. The frequency-dependent real part of the dielectric constant (ϵ') and imaginary part of the dielectric constant (ϵ'') can be calculated as follows:

$$\epsilon' = \frac{Cd}{\epsilon_0 A}, \tag{2}$$

$$\epsilon'' = \epsilon' \tan \delta, \tag{3}$$

where $\tan \delta$ is called as the dielectric loss tangent which is proportional to the loss of energy dissipated as heat from the applied field into the device. The variation of real (ϵ') and imaginary (ϵ'') components of dielectric constant as a function of frequency of LiF–WO₃ nano-composite thin films with different doping concentration of WO₃ at room temperature is shown in Fig. 4. Strong frequency dispersion can be seen at low frequency for all doping concentrations, and this dispersion increases with increase in doping concentration of up to 5%, whereas a frequency independent behavior can be seen above 100 Hz for all doping concentrations. The responsible factor for the dielectric constant of any material is polarization

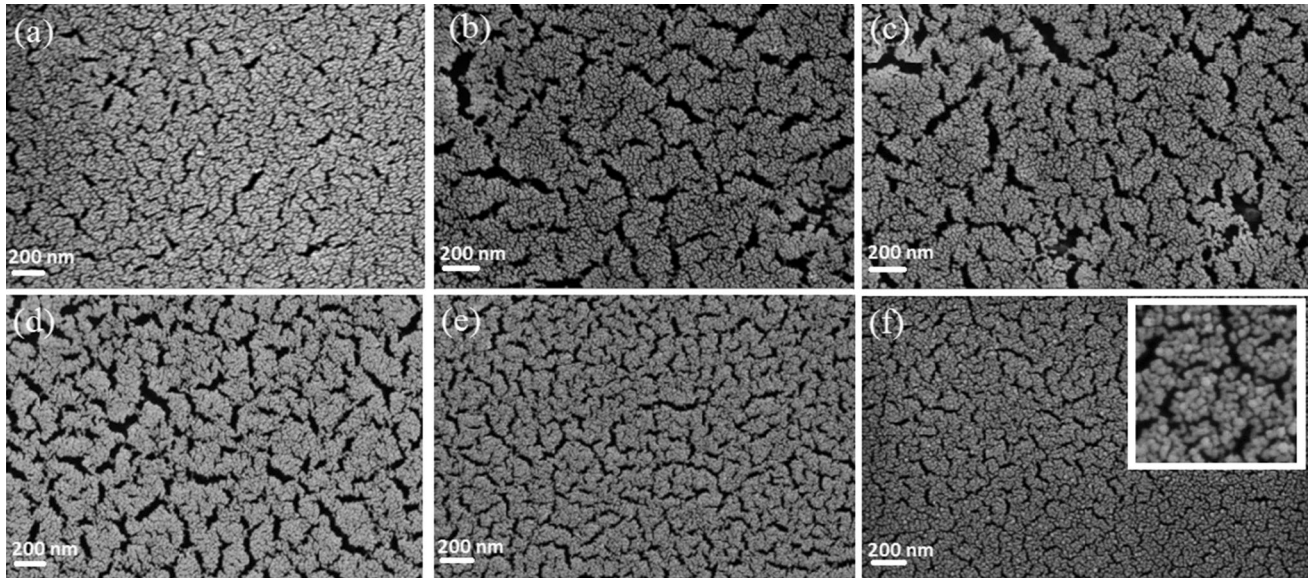


Figure 2 FESEM images of WO_3 -doped LiF nano-composite thin films at different concentrations of WO_3 : a 0%, b 1%, c 3%, d 5%, e 7%, f 10%.

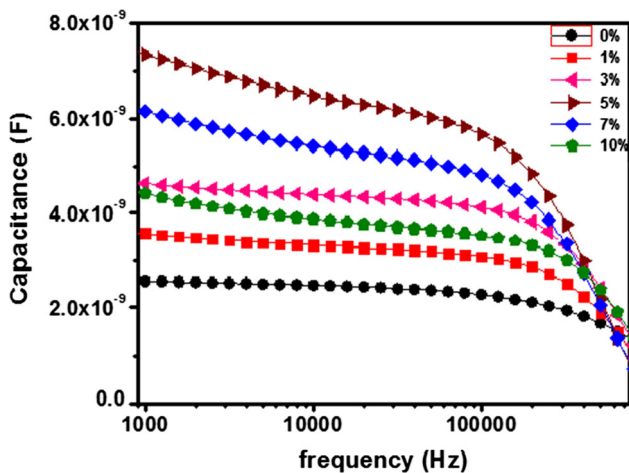


Figure 3 Capacitance as a function of frequency of WO_3 -doped LiF nano-composite thin films at different concentrations of WO_3 .

behavior shown by materials, namely bipolar, electronic, atomic, and space charge polarization which is operative at low frequencies [17]. The space charge polarization can be the reason behind frequency independent behavior of the curve. At high-frequency dipoles cannot orient themselves within time limit in the applied field direction due to which the interfacial polarization decreases with increase in frequency, results decreases the dielectric constant. Similarly at low frequencies, the dipoles follow the field rapidly and create maximum polarization value, resulting in high value of dielectric constant [18].

The frequency dependence behavior of the dielectric curve can be explained by Maxwell–Wagner model [19]. According to this model, it can be assumed that the dielectric material is made up of

Table 1 Fitted parameters of LiF– WO_3 nano-composite thin films obtained after the utilization of model equivalent circuit in Nyquist plots

Doping concentration (%)	Grain-boundary resistance, R_{gb} (Ω)	Bulk resistance, R_b (Ω)	Capacitance (nF)	Dielectric constant (k)
0	1.2×10^6	4.6×10^6	2.62	8.89
1	850000	3.9×10^6	3.56	12.08
3	550000	2.0×10^6	4.67	15.84
5	300000	1.4×10^6	7.42	25.2
7	450000	1.7×10^6	6.22	21.10
10	700000	2.4×10^6	4.44	15.06

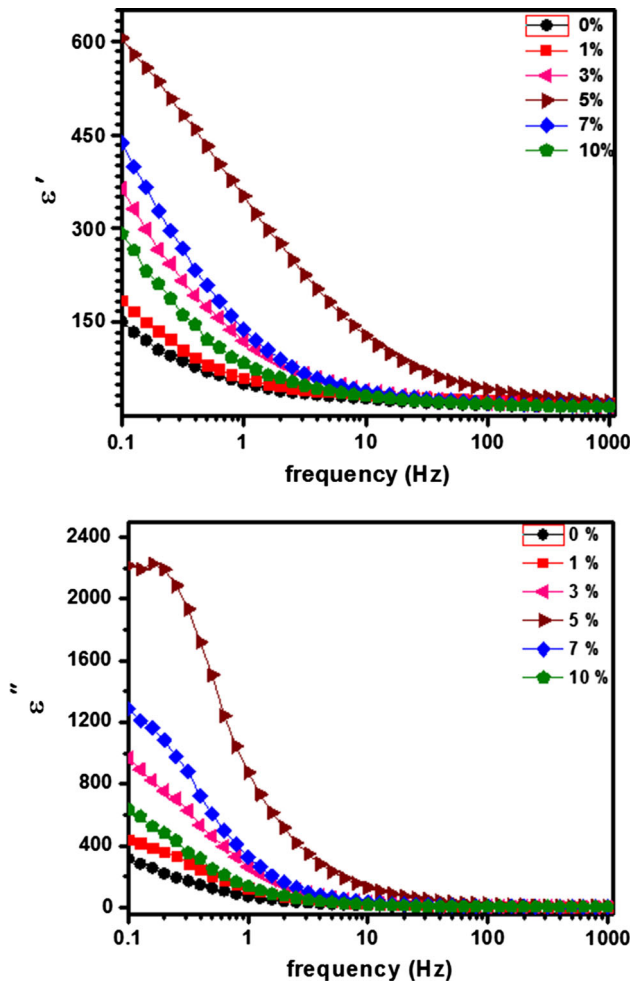


Figure 4 Variation of real (ϵ') and imaginary (ϵ'') components of dielectric constant as a function of frequency at room temperature.

grain and grain boundaries, where less conducting grain boundaries situated between two highly conducting grains. When an external electric field is applied to the dielectric material, the electric charges can easily travel through the grains, but it cannot cross grain boundaries and gets accumulated on grain boundaries and create large polarization in the form of high dielectric constant at low frequencies.

The electrical and dielectric properties of materials can be investigated by the complex impedance analysis technique. This technique provides us the capability to find out the overall electrical properties contribution, originated by grain (bulk), grain boundary or polarization phenomenon in a material [20]. Figure 5 shows the Nyquist plots of LiF–WO₃ nano-composite thin films for different doping concentrations of WO₃ over a wide range of frequency at room temperature. The characterization of an

impedance spectrum can be characterized by a semicircular arc. The appearance of a single semicircle indicates that the electrical process obeys a single relaxation mechanism [21]. If a semicircular arc comes at high frequency, then it represents a bulk contribution, whereas the intermediate frequency semicircle arc represents a grain-boundary contribution. The value of interception of the semi circular arc with the real axis (Z') gives us an estimate value of bulk resistance (R_b) of the material [22]. From Fig. 5, it can be observed that the size of semicircular arc decreases with increase in WO₃ doping concentration up to 5% and then it increases again. Hence, the size of the semicircles depends on the resistive responses of the material. It has also been observed from Fig. 5 that the impedance plot consists of depressed semi-circular and the center of arc lies below the real axis that shows the presence of a non-Debye type of relaxation phenomenon in the film and this behavior indicates that there is a distribution of relaxation time instead of a single relaxation time in the film.

The fitting of the Nyquist plot for all doping concentration is done by z-view software, and the best fit is obtained when employing an equivalent circuit formed by a parallel combination of resistance R_1 (bulk resistance R_b) and capacitance C_1 (bulk capacitance C_b) in series with a parallel combination of resistance R_2 (grain-boundary resistance R_{gb}) and capacitance C_2 (grain-boundary capacitance C_{gb}). The equivalent configuration is of the type $[(R_1 || C_1) + (R_2 || C_2)]$, as shown in the inset of Fig. 5. The

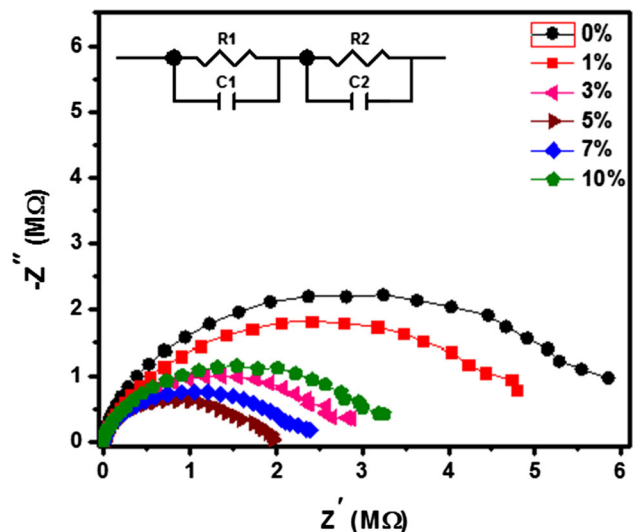


Figure 5 Nyquist plot of LiF–WO₃ nano-composite thin films at room temperature.

calculated parameters by fitting and the calculated dielectric constant using capacitance are given in Table 1.

Figure 6 shows the imaginary part of the impedance (Z'') as a function of frequency (loss spectrum) of LiF–WO₃ nano-composite thin films with different doping concentration of WO₃ at room temperature. The characterization of loss spectrum is done by appearance of broad peak at a particular frequency, also known as relaxation frequency. Only one electrical response can be seen in Fig. 6, and this may be due to the grains boundary contribution in the film [23]. For all concentrations, the electrical response reduces with the increase in doping concentration up to 5% and then it increases again. The grain response is expected to be appeared at high-frequency regions, which are limited to our frequency regions of investigations. It can be seen that the peaks pattern is asymmetric in loss spectrum and their positions shifted toward the higher-frequency region with increase in doping concentration of WO₃ up to 5%. The peak broadening suggests a spread of the relaxation time [24].

Figure 7 shows the real part of the impedance (Z') as a function of frequency of LiF–WO₃ nano-composite thin films with different doping concentration of WO₃ at room temperature. It is observed that the magnitude of Z' (i.e., resistance) decreases with increase in WO₃ doping concentration up to 5% and after that increases again. Hence decrease in magnitude of Z' up to 5% doping can be the possible factor for the increase in the ac conductivity. It can also be

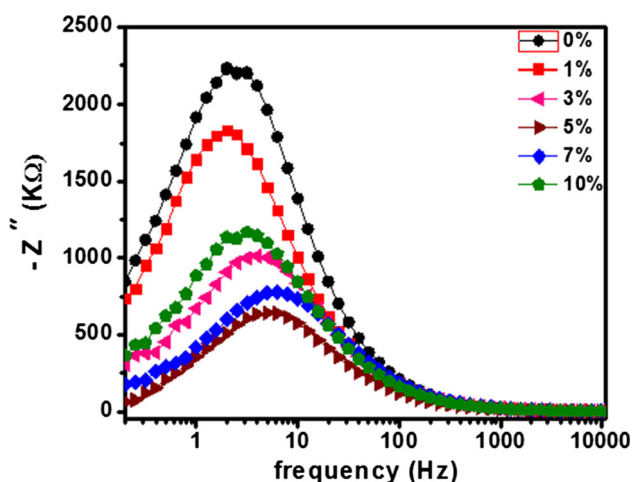


Figure 6 Imaginary part of the impedance (Z'') as a function of frequency at room temperature.

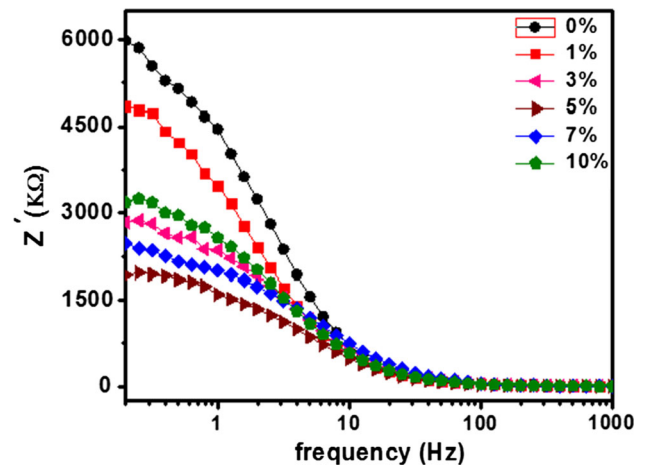


Figure 7 Real part of the impedance (Z') as a function of frequency at room temperature.

seen that the Z' values for all the concentrations merge in the higher-frequency region (≥ 100 Hz). This may happen due to reduction in barrier properties of the material with the rise in concentration results releases space charges and this may enhance the ac conductivity of the material at higher frequencies [25, 26].

The electrical modulus analysis of any material helps us to study the parameters such as electrical conductivities, electrode polarization, relaxation time, grain and the grain-boundary conduction effect of the material. The complex electric modulus, $M^*(\omega)$, is defined as the inverse of the complex permittivity, $\varepsilon^*(\omega)$:

$$M^* = M' + iM'' = 1/\varepsilon^*, \quad (4)$$

where M' is the real part of the electric modulus and can be calculated by using following equation:

$$M' = \varepsilon' / (\varepsilon'^2 + \varepsilon''^2), \quad (5)$$

and M'' is the imaginary part of the electric modulus and can be calculated as follows:

$$M'' = -\varepsilon'' / (\varepsilon'^2 + \varepsilon''^2), \quad (6)$$

Figure 8 shows the variation of the real (M') part of the dielectric modulus as a function of frequency of LiF–WO₃ nano-composite thin films with different doping concentration of WO₃ at room temperature. It can be seen that M' is having very low value at the low-frequency region and then there is a sigmoidal increase in the value of M' with increasing frequency. A continuous dispersion can be seen in the curve with increasing frequency which may be due to an

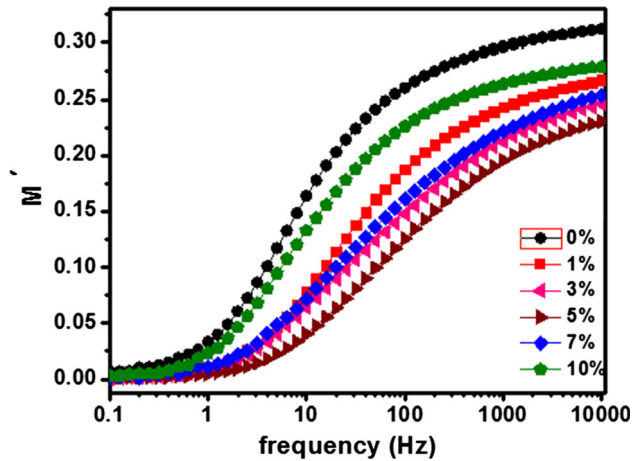


Figure 8 Variation of the real (M') part of the dielectric modulus as function of frequency at room temperature.

induced electric field driven short-range mobility of charge carriers [22].

Figure 9 shows the variation of the imaginary (M'') part of the dielectric modulus as a function of frequency of LiF-WO₃ nano-composite thin films with different doping concentration of WO₃ at room temperature. This curve is characterized by a peak appearing at a particular frequency. It can also be seen that the magnitude of the peaks and peak position shifts toward the high-frequency side with increase in doping concentration up to 5%. The M'' peak appearing at the low-frequency side represents the range of frequencies in which charge carriers can travel from one site to the neighboring site over a long distance. The M'' peak appearing at the high-frequency side indicates the frequency range in which the charge carriers cannot cross their potential

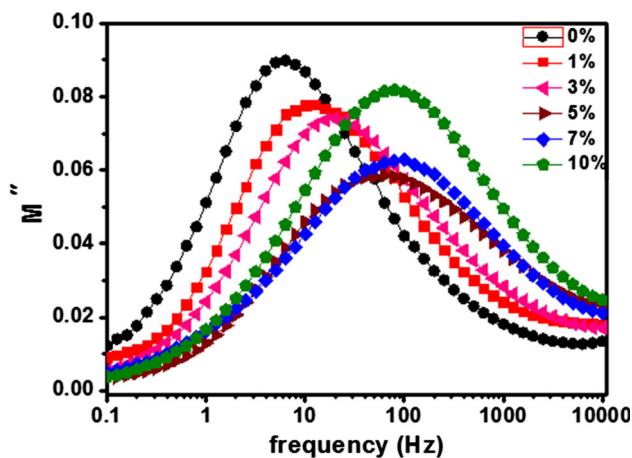


Figure 9 Variation of the imaginary (M'') part of the dielectric modulus as function of frequency at room temperature.

wells and their motion could be within the well [24]. Therefore, long-range to the short-range mobility of charge carrier transition can be seen in our investigation with increase in frequency. The peak broadening with different time constant indicates the spread of relaxation time, and hence a non-Debye type of relaxation is observed in the material [27].

Figure 10 shows the variation of dielectric loss ($\tan \delta$) as a function of frequency of LiF-WO₃ nano-composite thin films with different doping concentration of WO₃ at room temperature. The generation of heat in the form of energy loss after applying electric field can be measured as a dielectric loss tangent. The loss spectra characterized by peak appearing at a particular frequency, which suggest the presence of relaxing dipoles in the films. The dielectric loss of the film increases with increase in doping concentration up to 5% at low frequency. It can also be seen that the dielectric loss of the film has been decreased exponentially with increasing frequency and showed the frequency independent behavior at higher frequency. This may happen due to the orientation of dipole polarization which follows the electric field at lower frequencies resulting high dielectric loss. Similarly, at higher frequencies, the dipole response is limited and the dielectric loss decreases [28, 29].

The loss tangent behavior can also be explained by Koop’s model [30]. According to this model, at lower frequency grain boundaries play a dominant role due to which material shows high resistivity; hence, the electrons need much more energy to travel from one

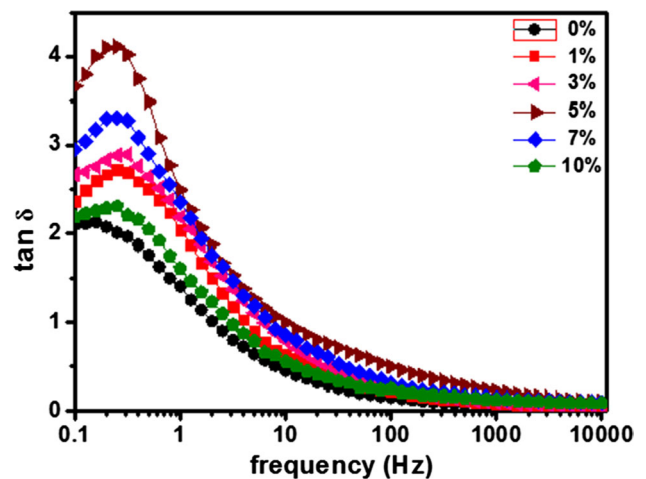


Figure 10 Variation of dielectric loss ($\tan \delta$) as a function of frequency at room temperature.

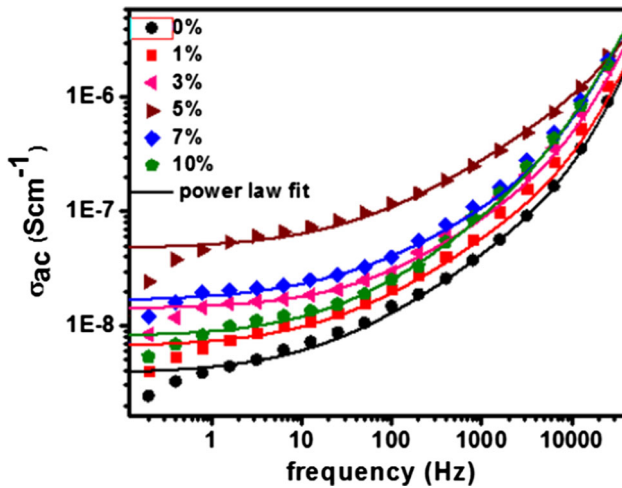


Figure 11 Dotted curve denotes the experimental data for the variation of ac conductivity as a function of frequency. The continuous solid line denotes the fit of experimental data to double exponential power law.

conducting grain to another. So, high energy dissipation can be seen at the low-frequency region. At high frequency, grains play a dominant role due to which material shows low resistivity. Therefore, less energy is required for the electrons to travel from one conducting grain to another resulting loss tangent decrease.

The AC electrical conductivity (σ_{ac}) of the prepared sample has been calculated from the following equation:

$$\sigma_{ac} = \omega \epsilon' \epsilon_0 \tan \delta, \quad (7)$$

where $\omega (= 2\pi f)$ is the angular frequency and f is the applied frequency. Figure 11 shows the log–log scale plot of the variation of calculated ac conductivity as a function of frequency of LiF-WO₃ nano-composite thin films with different doping concentration of WO₃ at room temperature. It can be seen that at low frequencies ac conductivity show a frequency independent plateau and at the higher frequencies it shows dispersion. A small deviation in the plateau

region can be seen at low frequencies which is the evidence of electrode polarization effect on the curve. The ideal model to fit experimental conductivity data is Jonscher's universal power law [31, 32]

$$\sigma(\omega) = \sigma_0 + A\omega^n, \quad (8)$$

where σ_0 is the dc conductivity, the exponent n can have a value between zero and one, and mobile ions and lattice interaction can be found out with this value, whereas A determines the strength of polarizability. However, this model does not fit to our data; hence, we have used double exponential power law [jump relaxation model (JRM)] [33, 34] to fit the data.

$$\sigma_{ac}(\omega) = \sigma_{dc}(0) + A_1\omega^{n_1} + A_2\omega^{n_2}, \quad (9)$$

where $\sigma_{dc}(0)$ corresponds to the long-range translation hopping which gives the DC conductivity of the systems. The second factor $A_1\omega^{n_1}$ is used for the short-range translational hopping motion, where the exponent n_1 values should be between zero and one. The third factor $A_2\omega^{n_2}$ is associated with a localized hopping motion and the exponent n_2 values should be between one and two.

According to jump relaxation model, dc conductivity contribution at low frequencies can be considered because of the successful transition of an ion from one site to its neighboring vacant site. At higher frequencies, the forward–backward hopping probability of an ion to its initial site increases due to the availability of short time periods and this can be the responsible factor for the high-frequency conductivity dispersion [35]. The values of $\sigma_{dc}(0)$, A_1 , A_2 , n_1 and n_2 obtained by the jump relaxation model are tabulated in Table 2. From the table, it is clear that the dc conductivity increases with increase in doping concentration up to 5%.

Table 2 Fitted ac conductivity parameters of x wt% WO₃-doped LiF nano-composite thin films by double exponential power law

X wt% doping (%)	$\sigma_{dc}(0)$, (S cm^{-1})	A_1	A_2	n_1	n_2
0	3.9×10^{-9}	5.5×10^{-10}	3.8×10^{-15}	0.61	1.85
1	6.5×10^{-9}	8.4×10^{-10}	5.6×10^{-15}	0.59	1.83
3	1.4×10^{-8}	9.6×10^{-10}	9.4×10^{-15}	0.58	1.82
5	4.7×10^{-8}	4.5×10^{-9}	1.5×10^{-14}	0.57	1.73
7	1.6×10^{-8}	2.02×10^{-9}	7.09×10^{-14}	0.59	1.75
10	8.05×10^{-9}	9.04×10^{-10}	7.5×10^{-14}	0.60	1.76

Conclusion

In conclusion, we have fabricated a MIM device of LiF–WO₃ nano-composite thin films and its electrical and dielectric properties of the films have been investigated. The analysis of the dielectric nature of the doped films was done by the space charge polarization and Maxwell–Wagner model. The appearance of semicircle arc shows the characteristic of impedance spectrum, and the electrical properties of the films exhibit both grain and grain-boundary conduction which showed relaxation in the films to be of non-Debye type. The study of electrical transport process has been done by modulus analysis, and this indicates non-Debye type conductivity relaxation in the film which is also evidenced by the impedance spectroscopy. With the help of Koop's model, the loss tangent analysis has been performed. The frequency dependent of ac conductivity follows double exponential power law feature and the low-frequency dispersion indicating the presence of electrode polarization phenomena in the materials. From all the analysis, we can conclude that the electrical and dielectric properties of LiF–WO₃ nano-composite thin films have been modified with doping concentration of up to 5%.

Acknowledgements

The authors gratefully recognize the financial support from University Grants Commission (UGC) and CSIR network Project NWP-55 (TAPSUN) for funds.

Compliance with ethical standards

Conflict of interest All authors declare that they have no conflict of interest.

References

- Peng B, Ren X, Wang Z et al (2014) High performance organic transistor active-matrix driver developed on paper substrate. *Sci Rep* 4:6430
- Fukuda K, Takeda Y, Mizukami M et al (2014) Fully solution-processed flexible organic thin film transistor arrays with high mobility and exceptional uniformity. *Sci Rep* 4:3947
- Lee S, Reuveny A, Reeder J et al (2016) A transparent bending-insensitive pressure sensor. *Nat Nanotechnol* 11:472–478
- Nawrocki RA, Matsuhisa N, Yokota T, Someya T (2016) 300-nm Imperceptible, ultraflexible, and biocompatible e-skin fit with tactile sensors and organic transistors. *Adv Electron Mater* 2:1500452
- Fukuda K, Takeda Y, Yoshimura Y et al (2014) Fully-printed high-performance organic thin-film transistors and circuitry on one-micron-thick polymer films. *Nat Commun* 5:4147
- Yamashita Y (2009) Organic semiconductors for organic field-effect transistors. *Sci Technol Adv Mater* 10:24313
- Li J, Liu D, Miao Q, Yan F (2012) The application of a high-*k* polymer in flexible low-voltage organic thin-film transistors. *J Mater Chem* 22:15998
- Xu W, Rhee S-W (2009) Low-operating voltage organic field-effect transistors with high-*k* cross-linked cyanoethylated pullulan polymer gate dielectrics. *J Mater Chem* 19:5250
- Tsai T-D, Chang J-W, Wen T-C, Guo T-F (2013) Manipulating the hysteresis in poly(vinyl alcohol)-dielectric organic field-effect transistors toward memory elements. *Adv Funct Mater* 23:4206–4214
- Faraji S, Danesh E, Tate DJ et al (2016) Cyanoethyl cellulose-based nanocomposite dielectric for low-voltage, solution-processed organic field-effect transistors (OFETs). *J Phys Appl Phys* 49:185102
- Ma L, Yang Y (2004) Unique architecture and concept for high-performance organic transistors. *Appl Phys Lett* 85:5084–5086
- Luo X, Du L, Yao B et al (2015) Operational dynamics and architecture dependence of double-gate OFETs with balanced top and bottom channel characteristics. *J Mater Chem C* 3:7336–7344
- Rao MC, Hussain OM (2011) Growth and characterization of vacuum evaporated WO₃ thin films for electrochromic device application. *Res J Chem Sci* 1(7):92–95
- Mäntymäki M, Hämäläinen J, Puukilainen E et al (2013) Atomic layer deposition of LiF thin films from Lithd and TiF 4 precursors. *Chem Vap Depos* 19:111–116
- Ozkan E, Lee S-H, Tracy CE et al (2003) Comparison of electrochromic amorphous and crystalline tungsten oxide films. *Sol Energy Mater Sol Cells* 79:439–448
- Hutchins MG, Abu-Alkhair O, El-Nahass MM, El-Hady KA (2006) Structural and optical characterisation of thermally evaporated tungsten trioxide (WO₃) thin films. *Mater Chem Phys* 98:401–405
- Ashok A, Somaiah T, Ravinder D et al (2012) Electrical properties of cadmium substitution in nickel ferrites. *World J Condens Matter Phys* 2:257–266
- Paul BK, Halder K, Roy D et al (2014) Dielectric switching above a critical frequency occurred in iron mullite composites

- used as an electronic substrate. *J Mater Sci: Mater Electron* 25:5218–5225. <https://doi.org/10.1007/s10854-014-2291-6>
- [19] Wagner KW (1973) Dissipation of energy under AC. *Am J Phys* 40:317
- [20] Das R, Sarkar T, Mandal K (2012) Multiferroic properties of Ba 2+ and Gd 3+ co-doped bismuth ferrite: magnetic, ferroelectric and impedance spectroscopic analysis. *J Phys Appl Phys* 45:455002
- [21] Shukla A, Choudhary RNP, Thakur AK (2009) Thermal, structural and complex impedance analysis of Mn4+ modified BaTiO₃ electroceramic. *J Phys Chem Solids* 70:1401–1407
- [22] Kaur B, Singh L, Reddy A et al (2016) AC impedance spectroscopy, conductivity and optical studies of Sr doped bismuth ferrite nanocomposites. *Int J Electrochem Sci* 11:4120–4135
- [23] Thakur S, Rai R, Sharma S, Tiwari A (2016) Study the influence of different mol% BLTMNZ doping on KNLN ceramics by using the XRD and impedance spectroscopy. *Adv Mater Lett* 7:29–35
- [24] Tahri T, Hamdaoui N, Omri A et al (2016) Study of electrical and dielectric properties of CaMn_{0.6}Fe_{0.4}O_{2.8} perovskite. *J Mater Sci: Mater Electron* 27:10525–10531. <https://doi.org/10.1007/s10854-016-5143-8>
- [25] Panda N, Parida BN, Padhee R, Choudhary RNP (2015) Structural, dielectric and electrical properties of the Ba₂-BiNbO₆ double perovskite. *J Mater Sci: Mater Electron* 26:3797–3804. <https://doi.org/10.1007/s10854-015-2905-7>
- [26] Das R, Gupta K, Jana K et al (2016) Preparation, characterization and dielectric, AC conductivity with electrochemical behavior of strontium zirconate. *Adv Mater Lett* 7:646–651
- [27] Kim JS (2001) Electric modulus spectroscopy of lithium tetraborate (Li₂B₄O₇) single crystal. *J Phys Soc Jpn* 70:3129–3133
- [28] Halder K, Roy D, Das S (2015) A comparative electrical study of nano-crystalline mullite with low dielectric loss due to incorporation of tungsten and molybdenum ion: their uses in electronic industries. *J Mater Sci: Mater Electron* 26:5803–5811. <https://doi.org/10.1007/s10854-015-3139-4>
- [29] Kazim Moosvi S, Majid K, Ara T (2016) Synthesis and characterization of PPY/K[Fe(CN)₃(OH)(en)] nanocomposite: study of photocatalytic, sorption, electrical, and thermal properties. *J Appl Polym Sci* 133:43487
- [30] Koops CG (1951) On the dispersion of resistivity and dielectric constant of some semiconductors at audio frequencies. *Phys Rev* 83:121–124
- [31] Jonscher AK (1977) The ‘universal’ dielectric response. *Nature* 267:673–679
- [32] Jonscher AK (1983) Dielectric relaxation in solids. Chelsea Dielectric Press, London
- [33] Peláiz-Barranco A, Gutiérrez-Amador MP, Huanosta A, Valenzuela R (1998) Phase transitions in ferrimagnetic and ferroelectric ceramics by ac measurements. *Appl Phys Lett* 73:2039–2041
- [34] Funke K (1993) Jump relaxation in solid electrolytes. *Prog Solid State Chem* 22:111–195
- [35] Pradhan DK, Choudhary RNP, Samantaray BK (2009) Studies of dielectric and electrical properties of plasticized polymer nanocomposite electrolytes. *Mater Chem Phys* 115:557–561